2024 IEEE International Conference on Robotics and Automation (ICRA 2024)
May 13-17, 2024. Yokohama, Japan

# Multi-modal jumping and crawling in an autonomous, springtail-inspired microrobot

Shashwat Singh[1,3], Zeynep Temel[3] and Ryan St. Pierre[1,2*]

***Abstract*— Springtails are tiny arthropods that crawl and jump. They jump by temporarily storing elastic energy in resilin elastic cuticular structures and releasing that energy to accelerate a tail, called a furca, propelling them in the air. This paper presents an autonomous, springtail-inspired microrobot that can crawl and jump. The microrobot has a mass of $980\,\mathrm{mg}$ and stands $13\,\mathrm{mm}$ tall, and has on-board sensing, computation, and power, enabling autonomy. The microrobot was designed with a super-elastic shape memory alloy (SMA) spring that is manually loaded to store elastic energy. The on-board sensing and computation triggers an actuator at the jump frequency range that unlatches the spring, launching the microrobot into the air at speeds up to $3.171\,\mathrm{m\,s^{-1}}$. At the same time, the microrobot is capable of crawling, when actuated at frequencies lower or higher than the jump frequency range, demonstrating autonomous multi-modal locomotion. This work opens up new pathways toward autonomy in multi-modal microrobots.**

## I. Introduction

Shrinking robots down to the size of insects comes with challenges in mobility, where obstacles encountered by robots are as large or larger than the robot itself [1]. One way to overcome large obstacles is through transitioning locomotion modes from crawling or walking to jumping. Springtails are tiny arthropods, less than $10\,\mathrm{mm}$ in body length, that can crawl and then use a spring-loaded tail to jump, even off of the surface of water [2], [3], [4], [5], [6]. Springtails have a highly specialized tail, called the furca, which latches under the springtail, then muscles contract to store elastic energy in resilin elastic cuticular structures that, upon unlatching, accelerates the tail to power the jump [7]. This system of springs and latches is called latch-mediated spring actuation (LaMSA). It is the mechanistic framework for most small jumping robots and insects [8], [9], [10], [11], and enables springtails to jump at speeds over $1.4\,\mathrm{m\,s^{-1}}$, depending on the species [2], [6].

Creating microrobots that can both jump and crawl is an issue to be resolved requiring actuators and mechanisms to be designed and utilized for each locomotion mode. The microrobot in [12] crawls with a wireless magnetic field at low frequencies. At high frequencies, the magnetic field inductively heats up the shape memory alloy (SMA) actuator, causing a rapid shape change and launching the microrobot.

This work was supported by the National Science Foundation (NSF) through award #2153327.

[1]Department of Mechanical and Aerospace Engineering, University at Buffalo, Buffalo, NY 14228, USA
[2]Department of Computer Science and Engineering, University at Buffalo, Buffalo, NY 14228, USA
[3]The Robotics Institute, Carnegie Mellon University, Pittsburgh, PA, 15213, USA
*ryans@buffalo.edu

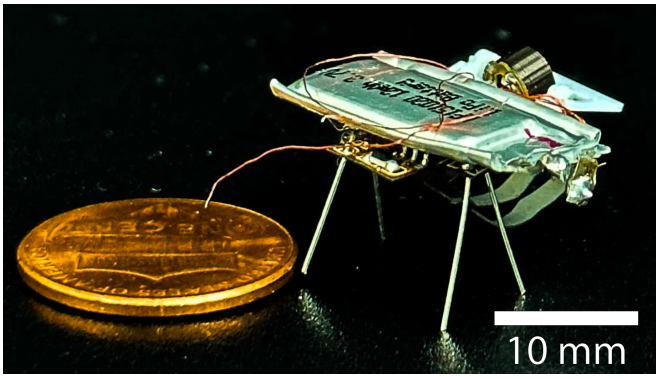


Fig. 1. A photograph of the springtail-inspired jumping microrobot standing next to a US penny. The microrobot is $13\,\mathrm{mm}$ tall and weighs $980\,\mathrm{mg}$ with on-board sensing, computation, and power, capable of autonomous operation.

The flea-sized microrobot in [13] uses a high voltage arc discharge to vibrate the cavity of the microrobot for crawling, and a rapid expansion of the cavity for jumping. The soft magnetic microrobot in [14] uses magnetic fields to crawl and deform the body of the robot to store elastic energy for jumping. SMA wire pairs are used in the microrobot in [15] to enable both jumping and crawling across rough terrain. Autonomy is still a challenge in these platforms.

Integrating on-board sensing, computation, and power is a problem to tackle for small robots [16]. One of the first demonstrations of an autonomous jumping microrobot used energetic silicon and an analog control circuit to launch a microrobot [17]. Other jumping microrobots have used wireless power transfer to enable autonomous operations. For example, the microrobot in [18] integrates photovoltaic cells to power an analog control circuit that controls the elastic energy loading into a spring to power the jump. The jumping microrobot in [19] uses wireless electromagnetic power transfer to heat SMA wires enabling the robot to jump. Bigger robots with body masses greater than $1\,\mathrm{g}$, integrating on-board sensing, computation, and power for autonomy in jumping have been demonstrated in various platforms, such as [20], [21], [22], [23].

Here, we present an autonomous $980\,\mathrm{mg}$ battery-powered microrobot (Figure 1) that not only jumps 45 times its body height but also crawls while consuming as low as $160\,\mathrm{mW}$ of power. The microrobot is equipped with a microcontroller for computation, a motor driver for powering the actuator, and a phototransistor for sensing. We detail the design and control of the microrobot in Sections II and III. The experiments

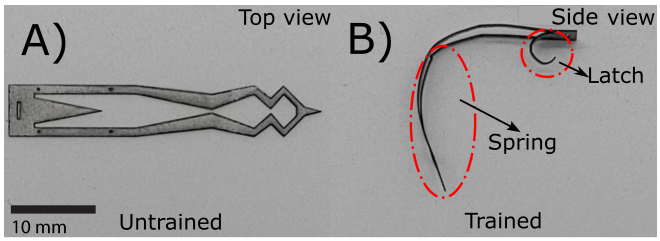


Fig. 2. The super-elastic shape memory alloy (SE-SMA) was used as the spring and latch of the microrobot. A) The 2-D design was cut out of a $0.19\,\mathrm{mm}$ thick sheet. B) The latch and the spring were trained through mechanical stress and heating shown by red markers.

used to characterize the jumping, crawling, and power consumption are detailed in Section IV, with the results shown in Section V. Finally, we compare our microrobot to other state-of-the-art jumping microrobots in Section VI, and discuss the implications of this microrobot in Section VII.

## II. Microrobot Design

Creating an autonomous jumping microrobot requires integrating a spring for storing elastic energy, a latch to block the release of the elastic energy until desired, an actuator to trigger the latch release with on-board computation, and power to trigger the actuator under a specific action. At the same time, to create a multi-modal autonomous microrobot, these same components needed to be used for crawling. The overall microrobot design and assembly are explained in the subsections below.

### A. Mechanical Design

The spring and latch are the key components for the mechanical structure to enable jumping. The spring and latch were made from a $0.19\,\mathrm{mm}$ thick sheet of super-elastic SMA (Nexmetal Corporation). The super-elastic SMA sheet was cut into the shape shown in Figure 2A using a UV laser cutter (LPKF ProtoLaser U4). Once the super-elastic SMA sheet was cut, the piece was trained into the shape shown in Figure 2B through both mechanical stress by holding the design under a vice to keep the shape and heating at $250\,^{\circ}\mathrm{C}$ for $20\,\mathrm{s}$ with forced hot air from a solder rework station. In this trained shape, the spring has an initial radius of curvature of $8.2\,\mathrm{mm}$, while the latch is trained with an even smaller radius of curvature of $1.9\,\mathrm{mm}$. The length of the untrained design is $37\,\mathrm{mm}$ which was chosen to withstand the bending force on tail without breaking due to high stress. The dimensions of the spring and latch, including their initial lengths and curvatures, were found empirically. These dimensions affect how much energy is stored in the system, and will utltimately dicate the jump performance of the microrobot. The spring was loaded manually, and placed on the latch, which holds the spring in place, blocking the release of elastic energy. The spring with latch has a mass of $134\,\mathrm{mg}$.

An electromagnetic hinge actuator measuring $10\,\mathrm{mm}$ by $10\,\mathrm{mm}$ with a nominal resistance of $62\,\Omega$ (Micronwings) was used to unlatch the spring. The cylindrical magnet in the

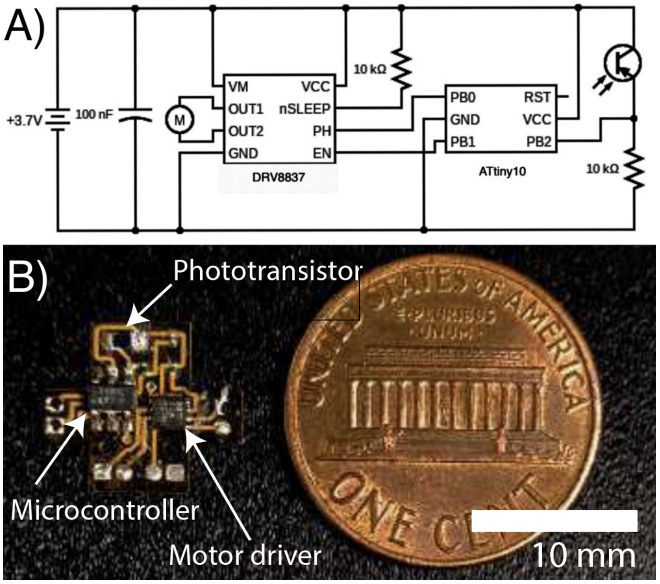


Fig. 3. A custom circuit board was designed for the microrobot. The schematic is shown in the top panel (A), and a photograph of the circuit board next to a US penny is shown in the bottom panel (B).

actuator was replaced with a higher grade (N52) cylindrical magnet measuring $2.2\,\mathrm{mm}$ in diameter and $2.5\,\mathrm{mm}$ in height was placed inside the actuator and secured with cyanoacrylate. The actuator with the replaced magnet has a mass of $180\,\mathrm{mg}$ total. The actuator was then mounted on top of the microrobot and secured with wire, such that the movable portion of the actuator impacts the tail.

Finally, four legs were included to allow the microrobot to stand with the spring underneath it. The legs were made from $0.35\,\mathrm{mm}$ thick and $10\,\mathrm{mm}$ long tin-plated copper-clad steel wire. The legs have a total mass of $74\,\mathrm{mg}$. The legs were then soldered to the two pairs of vias on both sides of the flexible printed circuit board (Figure 3B). While the legs provide structural support, they can also be used to reprogram the microrobot, since the vias that they are soldered to are also connected to the pins of the microcontroller.

### B. Electrical Design

The microrobot has a custom flexible printed circuit board (PCB) with electronics on-board for sensing, actuation, computation, and control. Figure 3A shows a schematic of the board. The board consists of ATtiny10, a low-power 8-bit AVR microcontroller (Atmel), an H-bridge motor driver (DRV8837, Texas Instruments), a $940\,\mathrm{nm}$ phototransistor (PT19-21B/TR8, Everlight), and with the actuator designated as the motor symbol. The custom PCB, shown in Figure 3B is shaped like a plus sign to reduce any unnecessary mass, and fits inside of a rectangular footprint of $6.1\,\mathrm{mm} \times 10.4\,\mathrm{mm}$. The populated board has a mass of $56\,\mathrm{mg}$.

The microrobot carries its own power supply in the form of a small lithium polymer battery, shown in the schematic in Figure 3A. The battery has a nominal voltage of $3.7\,\mathrm{V}$ and capacity of $12\,\mathrm{mA\,h}$. During operation, more than $12\,\mathrm{mA}$

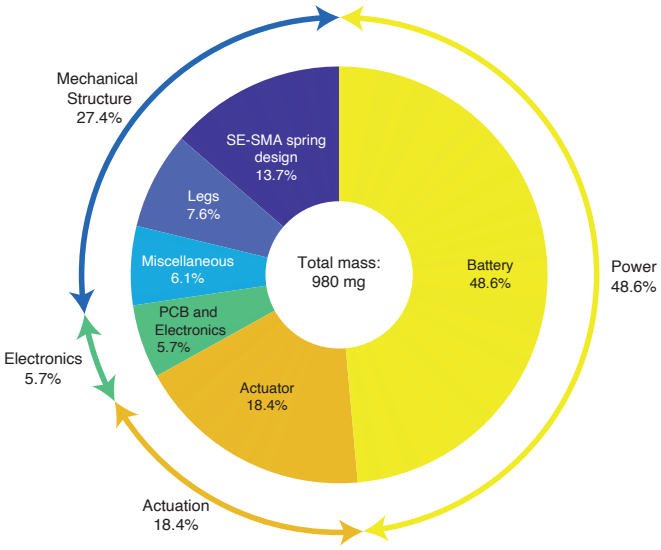


Fig. 4. The mass distribution of the microrobot. Nearly half of the mass of the microrobot is from the on-board power source.

is required to power the actuator. Therefore, the protection circuit, which limits the discharge rate of the battery, was removed to source more current for the actuator. This protection circuit removal comes with the added benefit of reducing the overall mass, making the final mass of the battery 476 mg.

### C. Assembly

The complete microrobot, shown in Figure 1, has a mass of 980 mg, and it is 13 mm tall in height, 21 mm long from front to back, when latched, and 23 mm wide from side to side. The complete mass distribution of the microrobot is shown in Figure 4. The on-board power source accounts for the majority of the mass of the microrobot at 48.6% of the total mass. The mechanical structure, including the spring and latch, legs, and additional components used for assembly alongside the actuator accounts for a nearly similar mass distribution of 45.8%. The electronics account for only 5.7% of the mass distribution.

## III. Control

Section II-B details the circuitry used to enable on-board sensing, computation, control, and ultimately autonomy, in the microrobot presented in this work. A simple control was implemented based on light sensed by the phototransistor. The microcontroller continuously checks the voltage from the phototransistor on the analog input on the microcontroller. If the voltage value from the phototransistor is above a pre-programmed chosen threshold, above the ambient light conditions, then the microcontroller triggers a pre-programmed behavior which sends an alternating out-of-phase on-off pulse to two digital outputs connected to the motor driver. This pre-programmed behavior applies a square wave centered around 0 V to the electromagnetic hinge actuator at frequencies between 5 Hz to 200 Hz. This control changes the polarity of the electromagnetic actuator with time, to allow for a large amplitude displacement of the actuator that impacts the spring to enable unlatching and crawling.

In this control, the voltage threshold of the phototransistor was chosen heuristically to be 1.37 V, which was chosen to be above the ambient lighting of a room. This threshold can be easily modified in software to be tuned to an even more specific trigger. At the same time, the alternating out-of-phase on-off pulses from the digital outputs of the microcontroller to the motor driver can be changed to different frequencies to accommodate different desired behaviors, detailed more in Section V. More sophisticated control can be implemented, however, the limited flash memory of the microcontroller must be accounted for. For example, different light intensity thresholds can be chosen to initiate different pre-programmed behaviors.

## IV. Experimental Setup

The jumping behavior of the microrobot was filmed with a high-speed camera (FASTCAM NOVA S12, Photron). The spring is manually loaded and placed onto the latch. The microrobot was placed in front of the camera and a light source illuminated the phototransistor to trigger the control. The autonomous jump was then filmed at 2000 fps with a tape measure in the frame for scale. To capture the entire jump sequence, from take-off to the apex of the jump height, a standard zoom lens (Nikkor 55-200mm f4-5.6G ED DX, Nikon) was used, captured video had a resolution 1024 px × 1024 px, corresponding to images of 0.53 m by 0.53 m.

To get a closer view of the unlatching process, the microrobot was filmed at a higher frame rate (10 000 fps) with a macro lens (Milvus 2/100M, Zeiss). Again, the microrobot spring had to be manually loaded and placed on the latch, then the phototransistor was illuminated to trigger the control. The captured video had a resolution 1024 px × 1024 px, corresponding to images of 70 mm by 70 mm with the macro lens.

The autonomous crawling behavior of the microrobot was recorded with the same standard zoom lens (Nikkor 55-200mm f4-5.6G ED DX, Nikon) and captured at 60 fps. The microrobot was filmed with both the spring latched and the spring unlatched. In both of these configurations, the phototransistor was illuminated by a constant light source to continue triggering the actuation, resulting in the microrobot crawling.

Finally, tethered experiments were performed to analyze the locomotion behavior and power consumed by the microrobot at different frequencies. The microrobot was tested by connecting the microrobot to a function generator (Tektronix AFG1062) and measuring the current using a source meter (KEITHLEY 2790). The function generator was set to output a square wave from −3.7 V to 3.7 V to emulate the commands sent by the microcontroller to the motor driver to power the actuator. The square wave frequency was swept from 5 Hz to 200 Hz in 5 Hz increments. All experiments were performed with both the spring latched and unlatched.

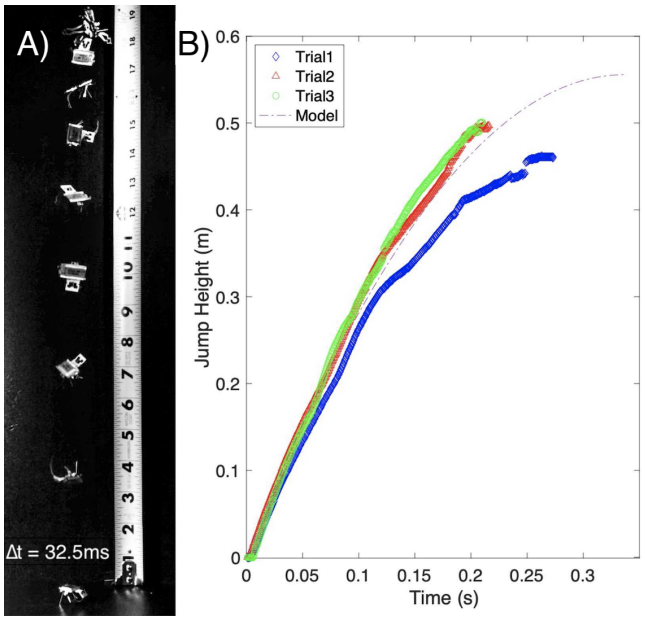


Fig. 5. A) Stills of the microrobot filmed at 2000 fps with 35.2 ms time difference were overlaid to create a composite image of the autonomous, battery-powered jump performance of the microrobot. B) The jump height over time was tracked over three trials and is plotted alongside a model of projectile motion (dashed line).

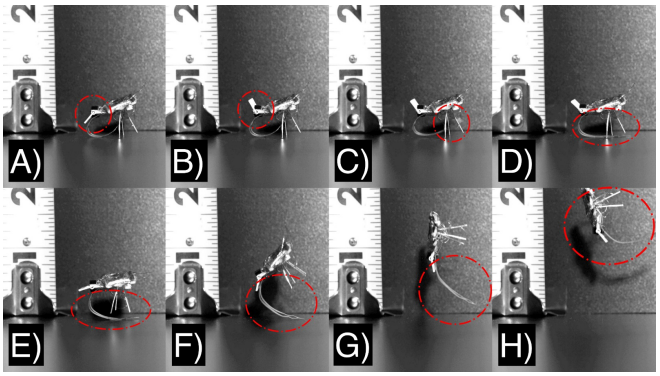


Fig. 6. A sequence of the microrobot unlatching and jumping. The microrobot was filmed at 10 000 fps, and keyframes with red markers showing A) no movement B) the actuator moving, C) spring unlatching, D) spring pushing against the ground, E) spring expansion, F) spring fully expanded, G) take-off from the ground, and H) ballistic motion. The entire sequence shown in these images occurs over 16.4 ms.

## V. Results

The autonomous jumping ability of the microrobot was filmed over three trials with high speed videography, as described in Section IV. Figure 5A shows a composite image of the microrobot jumping from the supplemental video. The jump of the microrobot was tracked a video tracking software (Tracker, physlets.org/tracker/), and the jump height over time is shown in Figure 5B. The take-off velocity is calculated from the tracked data as $3.171\,\mathrm{m\,s^{-1}}$, corresponding to $4.927\,\mathrm{mJ}$ of kinetic energy at take-off. The microrobot reached a maximum jump height of $48\,\mathrm{mm}$ in $374\,\mathrm{ms}$, corresponding to $0.461\,\mathrm{mJ}$ of gravitational potential energy at the apex. A total of $4.466\,\mathrm{mJ}$ is lost from take-off to the apex jump. This energy is most likely lost to rotational energy, as well as any dissipation from drag.

Alongside the experimental jumping data, a dashed line for a projectile motion model is plotted (Figure 5B). The model for projectile motion is given as

$$y(t) = v_{TO}t - \frac{1}{2}gt^2 \tag{1}$$

where $v_{TO}$ is the take-off velocity, and $g$ is the acceleration due to gravity. The model line over-predicts the apex jump height since this model only considers one-directional motion without any dissipation.

The unlatching sequence and ultimate take-off of the microrobot was filmed at a higher frame rate (10 000 fps) with a higher magnification lens. A sequence of images from the supplemental video is shown in Figure 6. During the unlatching sequence, the hinge actuator moves to either movement extreme, either impacting the microrobot or to the mechanical stop of the hinge actuator. At these extremes, the actuator comes to an abrupt stop, imparting energy to the system. The freely moving portion of the hinge actuator has a mass of $12\,\mathrm{mg}$ and is moved a linear distance of about $10\,\mathrm{mm}$. Given the range of frequencies test, from $5\,\mathrm{Hz}$ to $200\,\mathrm{Hz}$, the energy imparted by the hinge actuator to the microrobot is estimated between $15\,\mathrm{nJ}$ and $24\,\mu\mathrm{J}$. These packets of energy imparted by the hinge actuator to the rest of the microrobot structure result in the microrobot body deforming to dislodge the tail from the latch. In general, the spring unlatches after one to three cycles of movement from the actuator at $80\,\mathrm{Hz}$. The spring unlatches and recoils to contact the ground in $0.3\,\mathrm{ms}$. The spring then pushes against the ground to accelerate the microrobot in $6.7\,\mathrm{ms}$. Using the kinetic energy at take-off calculated earlier ($4.927\,\mathrm{mJ}$), and the time to take-off, this corresponds to $735\,\mathrm{mW}$ of power. Once the spring is fully extended, the microrobot takes off.

Figure 7 shows composite images of autonomous crawling of the microrobot with the spring both latched (Figure 7A) and unlatched (Figure 7B). For autonomous crawling, like jumping, the actuator moves to either movement extreme and imparts energy to the structure of the microrobot. This results in the body deforming moving the legs of the microrobot, resulting in the crawling through stick-slip friction. When the spring is latched, and the actuator moves but does not excite the structural dynamics of the microrobot where it could unlatch. Instead, the spring is kept loaded which would enable the microrobot to crawl and then jump. In Figure 7 the actuator was pulsed at $130\,\mathrm{Hz}$ for both the latched and unlatched configurations. When the spring is latched, the microrobot crawls $55\,\mathrm{mm}$ in $761\,\mathrm{s}$, an average velocity of $0.07\,\mathrm{mm\,s^{-1}}$. When the spring is unlatched, the microrobot crawls $66\,\mathrm{mm}$ in $297\,\mathrm{s}$, an average velocity of $0.22\,\mathrm{mm\,s^{-1}}$. The microrobot crawls at different speeds when latched and unlatched due to the different vibration modes of the entire microrobot body. When unlatched, the spring is cantilevered behind the microrobot, and allowed to vibrate freely compared to when the spring is latched. Examples of microrobot

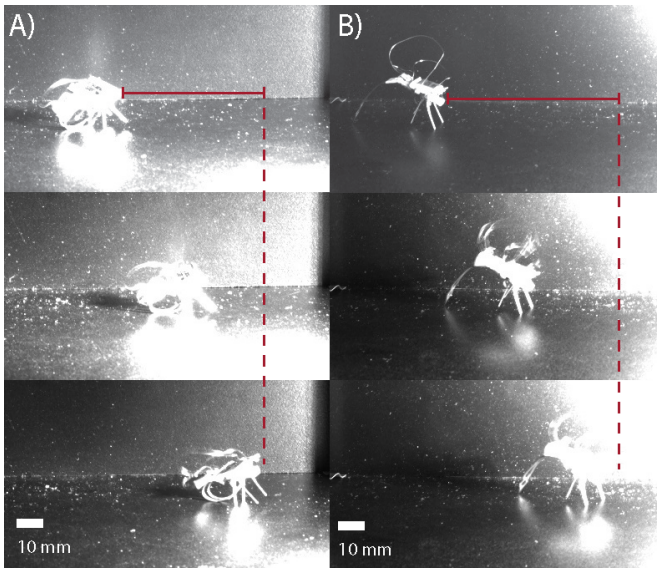


Fig. 7. A composite image of the microrobot crawling from left to right in the A) latched state and B) unlatched state. The microrobot crawling while latched (A) moves 55 mm over 761 s, and moves 66 mm over 297 s while unlatched (B).

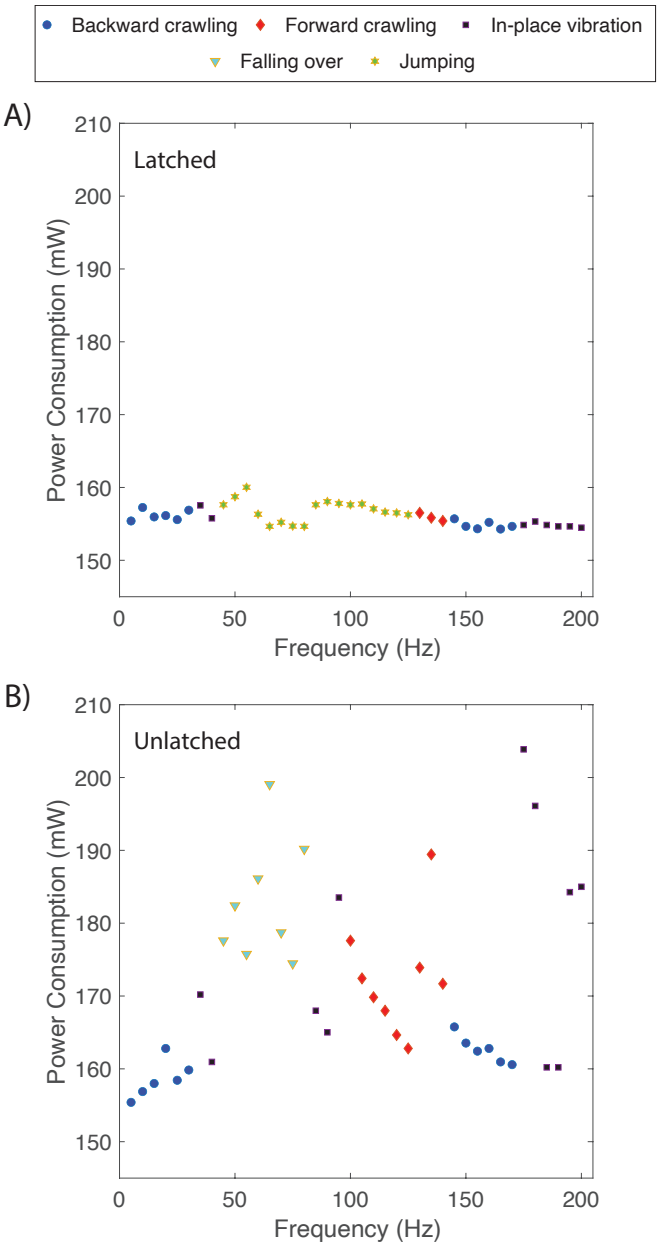


Fig. 8. The measured power consumption over different actuation frequencies when the microrobot is latched (A) and unlatching (B). The markers in each graph denote the locomotion mode observed at each actuation frequency when the microrobot is latched and unlatched.

crawling are shown in the supplemental video.

The power consumed and locomotion behavior of the microrobot is dependent on both the actuation frequency and whether the spring is latched or unlatched. Figure 8 plots the consumed power by the actuator with respect to the actuation frequency and distinguished the observed locomotion mode. Figure 8A plots the consumed power by the microrobot when the spring is latched. Generally, the microrobot consumes a similar power across all frequencies, between 154.29 mW and 160.2 mW. When the microrobot is latched, four distinct locomotion modes are observed depending on the actuation frequency. From 5 Hz to 30 Hz, and again from 145 Hz to 170 Hz, the microrobot crawls backward, opposite to the direction shown in Figure 7. The microrobot vibrates in place, and does not have an observable forward or background movement at 35 Hz to 40 Hz and again from 175 Hz to 200 Hz. The spring will unlatch and the microrobot will jump from 45 Hz to 125 Hz. Finally, forward crawling is observed from 130 Hz to 140 Hz.

Figure 8B plots the consumed power and observed locomotion mode when the microrobot is unlatched. When the microrobot is unlatched, the vibration mode of the entire body is different than when latched. This corresponds to different actuator dynamics, which consumes different power, depending on actuation frequency and body vibration. Similar to the latched state, the microrobot crawls backward from 5 Hz to 30 Hz and again from 145 Hz to 170 Hz, with similar consumed power. When unlatched, the microrobot will vibrate in place at three distinct regions, from 35 Hz to 40 Hz, from 85 Hz to 95 Hz, and from 175 Hz to 200 Hz, one additional frequency region compared to when the microrobot is latched. In these regions, the consumed power is higher, up to 199.06 mW from the differing actuator dynamics and overall body vibration. Since the spring is unlatched, the microrobot cannot jump, and instead, falls over when the microrobot would jump when latched, from 45 Hz to 80 Hz. The forward crawling region is expanded when the microrobot is unlatched, from 100 Hz to 140 Hz.

## VI. Comparison to other jumping microrobots

Figure 9 shows the take-off velocity vs. body mass of state-of-the-art jumping microrobots under 1 g. Take-off velocity was chosen as the comparable metric since the jump height would be easily influenced by the shape and take-off angle of any of the microrobots compared. Therefore,

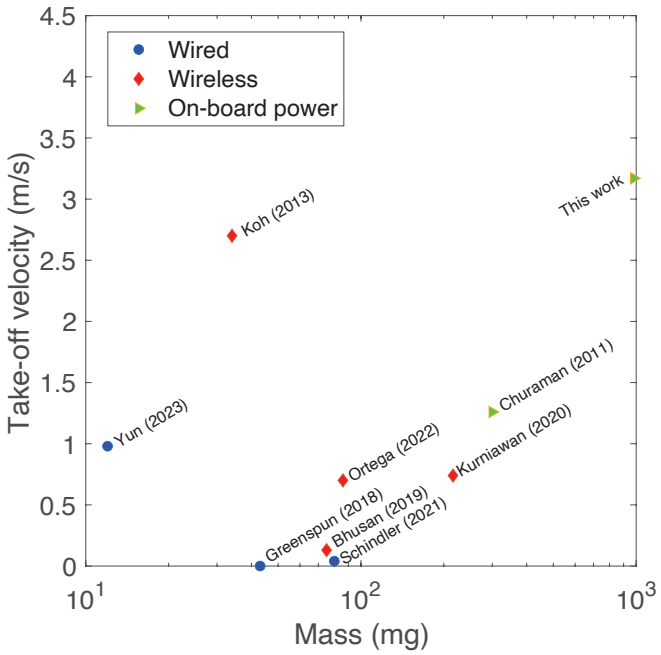


Fig. 9. The take-off velocity and mass of other state-of-the-art jumping microrobots under 1 g in body mass [6], [13], [17], [18], [19], [24], [25], [26].

take-off velocity provides a more uniform comparison, and provides a more accurate representation of the system energy for any of the microrobot systems. In this comparison, the markers show the microrobots that are tethered to power sources with or without wires and microrobots that have their own on-board power source. The majority of these jumping microrobots are tethered, either wired or wirelessly, to a power source. For example, the microrobots in [13], [24], [25] are physically tethered to a power source, the microrobots in [26], [6] are heated through a hot plate, the microrobot by Bhushan et al [18] has a photovoltaic cell on board, and the microrobot by Kurniawan et al [19] uses wireless power transfer through electromagnetic coils. Our microrobot and the microrobot by Churaman et al [17] have their own on-board energy sources to enable their jumping. Our microrobot has one of the highest take-off velocities of the reported and calculated velocities shown in Figure 9. The slightly larger robot from [27] (1.2 g) has a take-off velocity of $4\,\mathrm{m\,s^{-1}}$. Some design changes in our microrobot, where more energy is stored in the SE-SMA spring, could further increase our take-off velocity.

## VII. Conclusions

The microrobot presented in this work is capable of autonomous, multi-modal locomotion from jumping to crawling. The overall microrobot has a mass of $980\,\mathrm{mg}$ and is $13\,\mathrm{mm}$ tall in height, $21\,\mathrm{mm}$ long from front to back, when latched, and $23\,\mathrm{mm}$ wide from side to side. The microrobot has on-board sensing, computation, and power, enabling the autonomous operation of the microrobot. When jumping, the microrobot takes off with a velocity of $3.171\,\mathrm{m\,s^{-1}}$. This take-off velocity is comparable to other microrobots, shown in Figure 9, and even comparable to biological organisms and larger robots tabulated in [9] At take-off, the mechanical energy and power are $4.927\,\mathrm{mJ}$ and $735\,\mathrm{mW}$, respectively. This corresponds to a power density of $750\,\mathrm{W\,kg^{-1}}$, comparable to the power densities of biological and robotic jumpers tabulated in [9].

The design of the microrobot is fairly simple, consisting of a spring and latch laser cut from a single sheet of superelastic shape memory alloy. The spring and latch are trained to a curved shape, and then attached to a custom PCB. Then, an actuator and battery are attached on top. The source files required to create the microrobot are available on GitHub [28]. This allows the microrobot to be open-access and available to researchers and robot makers. The GitHub repository even includes a video to guide the assembly of the microrobot, and sample code for operating the microrobot.

The microrobot presented here utilized the structural vibrations of the whole body to enable multi-modal locomotion. The frequency dependence on locomotive behavior was observed for the microrobot, both when the spring was latched and unlatched. The overall design of the microrobot, including the dimensions of the spring and latch provides an opportunity to study the structural dynamics of the microrobot body to tune the frequencies of the transitions between different locomotive behaviors. This opens up a rich study to explore the trends and trade-offs between spring, latch, and overall body design as we look to make microrobots functional and autonomous in real-world settings.

Deploying microrobots outside of laboratory settings and into the real-world will come with engineering challenges detailed in [16]. This microrobot opens up new pathways to the eventual deployment of microrobots outside of laboratory settings. Here, the microrobot has on-board computation and is capable of multi-modal locomotion, meaning that with a more sophisticated, but still simple, sensing scheme and accompanying algorithm, the microrobot could crawl and then jump when approaching an obstacle. Future adaptations where the microrobot could reload the spring and jump multiple times would further increase the utility of jumping microrobots outside of laboratory settings.

## References

[1] M. Kaspari and M. Weiser, "The size–grain hypothesis and interspecific scaling in ants," *Functional ecology*, vol. 13, no. 4, pp. 530–538, 1999.

[2] E. Christian, "The jump of the springtails," *Naturwissenschaften*, vol. 65, no. 9, pp. 495–496, 1978.

[3] S. P. Hopkin, *Biology of the springtails:(Insecta: Collembola)*. OUP Oxford, 1997.

[4] S. Sudo, M. Shiono, T. Kainuma, A. Shirai, and T. Hayase, "The kinematics of jumping of globular springtail," *Journal of Aero Aqua Bio-mechanisms*, vol. 3, no. 1, pp. 85–91, 2013.

[5] S. Sudo, T. Kainuma, T. Yano, A. Shirai, and T. Hayase, "Jumps of water springtail and morphology of the jumping organ," *Journal of the Japanese Society for Experimental Mechanics*, vol. 15, no. Special_Issue, pp. s117–s124, 2015.

[6] V. M. Ortega-Jimenez, E. J. Challita, B. Kim, H. Ko, M. Gwon, J.-S. Koh, and M. S. Bhamla, "Directional takeoff, aerial righting, and adhesion landing of semiaquatic springtails," *Proceedings of the National Academy of Sciences*, vol. 119, no. 46, p. e2211283119, 2022.

[7] F. G. d. L. Oliveira, "On springtails (hexapoda: Collembola): a morphofunctional study of the jumping apparatus," *Frontiers in Zoology*, vol. 19, no. 1, pp. 1–22, 2022.

[8] S. Longo, S. Cox, E. Azizi, M. Ilton, J. Olberding, R. St. Pierre, and S. Patek, "Beyond power amplification: latch-mediated spring actuation is an emerging framework for the study of diverse elastic systems," *Journal of Experimental Biology*, vol. 222, no. 15, p. jeb197889, 2019.

[9] M. Ilton, M. S. Bhamla, X. Ma, S. M. Cox, L. L. Fitchett, Y. Kim, J.-s. Koh, D. Krishnamurthy, C.-Y. Kuo, F. Z. Temel, A. Crosby, M. Prakash, G. Sutton, R. Wood, E. Azizi, S. Bergbreiter, and S. N. Patek, "The principles of cascading power limits in small, fast biological and engineered systems," *Science*, vol. 360, no. 6387, p. eaao1082, 2018.

[10] A. Sakes, M. van der Wiel, P. W. Henselmans, J. L. van Leeuwen, D. Dodou, and P. Breedveld, "Shooting mechanisms in nature: a systematic review," *Plos one*, vol. 11, no. 7, p. e0158277, 2016.

[11] S. Patek, D. Dudek, and M. Rosario, "From bouncy legs to poisoned arrows: elastic movements in invertebrates," *Journal of Experimental Biology*, vol. 214, no. 12, pp. 1973–1980, 2011.

[12] D. Wang, F. Sui, W. Qiu, Y. Peng, M. Zhang, X. Wang, and L. Lin, "An untethered crawling and jumping micro-robot," in *2021 21st International Conference on Solid-State Sensors, Actuators and Microsystems (Transducers)*, pp. 353–356, IEEE, 2021.

[13] R. Yun, Z. Liu, J. Leng, J. Huang, Y. Cui, X. Yan, and M. Qi, "A 3.4-millimeter flea-sized robot with powerful jumping and fast crawling locomotion," *IEEE Robotics and Automation Letters*, vol. 8, no. 5, pp. 2868–2873, 2023.

[14] W. Hu, G. Z. Lum, M. Mastrangeli, and M. Sitti, "Small-scale soft-bodied robot with multimodal locomotion," *Nature*, vol. 554, no. 7690, pp. 81–85, 2018.

[15] D. Li, D. Niu, G. Ye, B. Lei, J. Han, W. Jiang, F. Luo, J. Chen, H. Liu, and B. Lu, "Crawling–jumping synergic bioinspired robots harnessing electroactive bistable actuators by adjusting mechanical responses and forces," *Applied Materials Today*, vol. 24, p. 101091, 2021.

[16] R. St. Pierre and S. Bergbreiter, "Toward autonomy in sub-gram terrestrial robots," *Annual Review of Control, Robotics, and Autonomous Systems*, vol. 2, pp. 231–252, 2019.

[17] W. A. Churaman, L. J. Currano, C. J. Morris, J. E. Rajkowski, and S. Bergbreiter, "The first launch of an autonomous thrust-driven microrobot using nanoporous energetic silicon," *Journal of Microelectromechanical Systems*, vol. 21, no. 1, pp. 198–205, 2011.

[18] P. Bhushan and C. Tomlin, "An insect-scale untethered laser-powered jumping microrobot," *arXiv preprint arXiv:1908.03282*, 2019.

[19] R. Kurniawan, T. Fukudome, H. Qiu, M. Takamiya, Y. Kawahara, J. Yang, and R. Niiyama, "An untethered 216-mg insect-sized jumping robot with wireless power transmission," in *2020 IEEE/RSJ International Conference on Intelligent Robots and Systems (IROS)*, pp. 7881–7886, IEEE, 2020.

[20] Z. Zhakypov, K. Mori, K. Hosoda, and J. Paik, "Designing minimal and scalable insect-inspired multi-locomotion millirobots," *Nature*, vol. 571, no. 7765, pp. 381–386, 2019.

[21] L. Tang, X. Wu, P. Liu, Y. Li, and B. Li, "The feedback trajectory control of a sma-driven miniature jumping robot," in *2022 International Conference on Robotics and Automation (ICRA)*, pp. 9769–9775, IEEE, 2022.

[22] Y. Wang, Q. Wang, M. Liu, Y. Qin, L. Cheng, O. Bolmin, M. Alleyne, A. Wissa, R. H. Baughman, D. Vella, and S. Tawfick, "Insect-scale jumping robots enabled by a dynamic buckling cascade," *Proceedings of the National Academy of Sciences*, vol. 120, no. 5, p. e2210651120, 2023.

[23] L. Tang, Y. Li, and B. Li, "Moobot: a miniature origami omnidirectional jumping robot with high trajectory accuracy," *IEEE Transactions on Industrial Electronics*, 2023.

[24] J. T. Greenspun and K. Pister, "First leaps of an electrostatic inchworm motor-driven jumping microrobot," in *Hilton Head Solid-State Sensors, Actuators, and Microsystems Workshop, Hilton Head Island, SC*, vol. 3, 2018.

[25] C. B. Schindler, H. C. Gomez, and K. S. Pister, "First jumps of a silicon microrobot with an energy storing substrate spring," in *2021 21st International Conference on Solid-State Sensors, Actuators and Microsystems (Transducers)*, pp. 349–352, IEEE, 2021.

[26] J.-S. Koh, S.-p. Jung, R. J. Wood, and K.-J. Cho, "A jumping robotic insect based on a torque reversal catapult mechanism," in *2013 IEEE/RSJ International Conference on Intelligent Robots and Systems*, pp. 3796–3801, IEEE, 2013.

[27] M. Noh, S.-W. Kim, S. An, J.-S. Koh, and K.-J. Cho, "Flea-inspired catapult mechanism for miniature jumping robots," *IEEE transactions on robotics*, vol. 28, no. 5, pp. 1007–1018, 2012.

[28] "Springtail Microrobot - GitHub Repository." `https://github.com/RobotFormAndFunction/Springtail_microrobot`, 2023.